Inflammation Research (2019) 68:1011–1024
https://doi.org/10.1007/s00011-019-01282-4

Inflammation Research

ORIGINAL RESEARCH PAPER

Tannic acid prevents macrophage-induced pro-fibrotic response in lung epithelial cells via suppressing TLR4-mediated macrophage polarization

Ayyanar Sivanantham[1] · Dhamotharan Pattarayan[1] · Nandhine Rajasekar[1] · Adithi Kannan[2] · Lakshmanan Loganathan[3] · Ramalingam Bethunaickan[4] · Santanu Kar Mahapatra[2] · Rajaguru Palanichamy[1] · Karthikeyan Muthusamy[3] · Subbiah Rajasekaran[1,5]

Received: 25 June 2019 / Revised: 27 August 2019 / Accepted: 29 August 2019 / Published online: 5 September 2019

Abstract

Background Polarized macrophages induce fibrosis through multiple mechanisms, including a process termed epithelial-to-mesenchymal transition (EMT). Mesenchymal cells contribute to the excessive accumulation of fibrous connective tissues, leading to organ failure. This study was aimed to investigate the effect of tannic acid (TA), a natural dietary polyphenol on M1 macrophage-induced EMT and its underlying mechanisms.

Materials First, we induced M1 polarization in macrophage cell lines (RAW 264.7 and THP-1). Then, the conditioned-medium (CM) from these polarized macrophages was used to induce EMT in the human adenocarcinomic alveolar epithelial (A549) cells. We also analysed the role of TA on macrophage polarization.

Results We found that TA pre-treated CM did not induce EMT in epithelial cells. Further, TA pre-treated CM showed diminished activation of MAPK in epithelial cells. Subsequently, TA was shown to inhibit LPS-induced M1 polarization in macrophages by directly targeting toll-like receptor 4 (TLR4), thereby repressing LPS binding to TLR4/MD2 complex and subsequent signal transduction.

Conclusion It was concluded that TA prevented M1 macrophage-induced EMT by suppressing the macrophage polarization possibly through inhibiting the formation of LPS-TLR4/MD2 complex and blockage of subsequent downstream signal activation. Further, our findings may provide beneficial information to develop new therapeutic strategies against chronic inflammatory diseases.

Keywords EMT · LPS · M1 macrophages · Mesenchymal cells · Tannic acid · TLR4

Introduction

In many chronic inflammatory diseases, fibrosis is the final pathological state and often culminates in organ failure. Activated fibroblasts/myofibroblasts are the primary effector

Responsible Editor: John Di Battista.

Electronic supplementary material The online version of this article (https://doi.org/10.1007/s00011-019-01282-4) contains supplementary material, which is available to authorized users.

✉ Subbiah Rajasekaran
rajasekarphd@gmail.com

[1] Department of Biotechnology, BIT-Campus, Anna University, Tiruchirappalli, Tamil Nadu, India

[2] Centre for Research in Infectious Diseases (CRID), School of Chemical and Biotechnology, SASTRA Deemed To Be University, Thanjavur, Tamil Nadu, India

[3] Pharmacogenomics and CADD Lab, Department of Bioinformatics, Alagappa University, Karaikudi, Tamil Nadu, India

[4] Department of Immunology, ICMR-National Institute for Research in Tuberculosis, Chennai, Tamil Nadu, India

[5] Department of Biochemistry, ICMR-National Institute for Research in Environmental Health, Kamla Nehru Hospital Building, Gandhi Medical College Campus, Bhopal, Madhya Pradesh, India

cells involved in the pathogenesis of fibrosis [1, 2]. The wound healing process becomes pathological when myofibroblasts persist and secrete excessive levels of extracellular matrix (ECM) proteins, resulting in substantial remodeling of the ECM and the formation of permanent scar [1, 3]. Although these myofibroblasts can be derived from a wide variety of cell types, it is believed that at least 30% of the total myofibroblast population are from the epithelial origin [3, 4]. The proposed mechanism involved in these phenomena is epithelial-to-mesenchymal transition (EMT). During EMT, polarized epithelial cells lose their epithelial properties, intercellular adhesions and gain fibroblast-like characteristics. These changes are accompanied by a reduction in the expression of epithelial markers such as E-cadherin (E-CAD) and a gain in the expression of mesenchymal markers such as N-cadherin (N-CAD) and vimentin (VIM) [5]. In response to inflammatory injury, EMT begins as a profibrogenic event to reconstruct tissues but ceases once the inflammation is attenuated. However, EMT can continue to respond to chronic inflammation that eventually leading to deterioration of normal tissue structure [6].

Among different inflammatory cellular components, macrophages have a crucial role and provide various soluble factors that promote the onset and progression of fibrosis by inducing multiple biological processes, including EMT [7, 8]. Further, macrophages can acquire distinct phenotypes and biological functions depending on the stimuli [9]. The classically activated M1 macrophage (pro-inflammatory) is induced by lipopolysaccharides (LPS) alone or in combination with interferon-γ (IFN-γ), while alternatively activated M2 macrophage (anti-inflammatory) is induced by interleukin (IL)-4 and -13. However, emerging evidence demonstrated that both pro-inflammatory and anti-inflammatory macrophages may participate in the pro-fibrotic processes such as EMT [7, 10].

Tannins are water-soluble polyphenols and widely exist in several common human foods, including vegetables, fruits, nuts, cereals, wine, and green tea [11]. Though tannins have been characterized into four major groups, tannic acid (TA) and ellagitannins are known to be the most widespread types [12]. The chemical formula of TA is $C_{76}H_{52}O_{46}$ and is a mixture of five galloyl esters and a glucose [12]. Further, TA has been shown to possess anti-fibrotic [13, 14], anti-inflammatory [15], anti-mutagenic [16], anti-carcinogenic [17], and anti-oxidant effects [18].

In the present study, we investigated the effect of TA on M1 macrophage-induced pro-fibrotic response in lung epithelial cells. We found that TA treatment suppressed macrophage polarization and macrophage secreted soluble factors, which eventually reduced M1-CM (conditioned-medium)-induced EMT in epithelial cells. Further, this study suggested that TA may directly bind to toll-like receptor 4 (TLR4), thereby repressing LPS binding to TLR4/MD2 complex and subsequent signal transduction. Hence, this study provides further insights regarding the role of TA in attenuation of inflammation-induced EMT and supports its therapeutic benefits in inflammation-mediated diseases including fibrosis.

Materials and methods

Reagents and chemicals

TA, LPS, and LPS-FITC (Fluorescein isothiocyanate) were purchased from Sigma-Aldrich (St. Louis, MO, USA). The cell culture mediums, antibiotic and antimycotic solutions were obtained from HiMedia Laboratories (Mumbai, Maharashtra, India). TRIzol reagent (Life Technologies, Carlsbad, CA, USA), High Capacity cDNA Reverse Transcription Kit (Applied Biosystems, Vilnius, Lithuania), SYBR green master mix (Applied Biosystems, Vilnius, Lithuania), and Radioimmunoprecipitation assay buffer (RIPA buffer) (Thermo Scientific, Rockford, IL, USA) were purchased. Sandwich-ELISA kit for the detection of mouse cytokines was purchased (R&D Systems, Minneapolis, MN, USA). Antibodies specific for E-CAD, N-CAD, CLDN (Claudin), VIM, phospho-ERK1/2 (Thr202/Tyr204) (Extracellular signal–regulated kinases1/2), phospho-p38 (Thr180/Tyr182), phospho-NF-kB-p65 (Ser536) (Nuclear Factor kappa-light-chain-enhancer of activated B cells), total-ERK1/2, total-p38, total-NF-kB, and HRP (horseradish peroxidase)-conjugated secondary antibodies (mouse and rabbit) were purchased from Cell Signaling Technology (Danvers, MA, USA). TLR4 (BD Biosciences, Franklin Lakes, NJ, USA), MD2 (Lymphocyte antigen 96) (Novus Biologicals, Centennial, CO, USA), and tubulin (Sigma-Aldrich, St. Louis, MO, USA) antibodies were purchased. Recombinant mouse TLR4 (Creative BioMart Inc, Shirley, NY, USA) and protein A/G plus-Agarose beads (Santa Cruz Biotechnology Inc, Dallas, Texas, USA) were purchased. The ECL (Enhanced chemiluminescence) detection kit was purchased from Thermo Scientific (Rockford, IL, USA). All the other chemicals used were of analytical grade unless otherwise stated.

Cell culture and preparation of M1-conditioned medium from macrophages

Raw 264.7 (murine macrophage cell line) and A549 (human adenocarcinomic alveolar epithelial cell line) were maintained in DMEM (Dulbecco's Modified Eagle Medium) supplemented with 10% fetal bovine serum (FBS), and antibiotic and antimycotic solutions. THP-1 (human macrophage cell line) cells were cultured in RPMI (Roswell Park Memorial Institute medium) 1640 medium. All cell lines were cultured in a humidified chamber at 37 °C with 5%

CO_2. The cells were frozen at an early passage and cultured for a maximum of six passages. For the induction of M1 polarization in RAW 264.7 cells, 100 ng/mL of LPS was used in serum-free medium for 24 h. In THP-1 cells, cells were first treated with 100 nmol of phorbol 12-myristate 13-acetate (PMA) for 48 h, followed by exposure to LPS in serum-free medium for 24 h. At the end of LPS treatment, the cell culture supernatant (considered as M1-CM) was then collected by centrifugation, filtered, and used immediately or stored at − 80 °C until further use. To observe the influence of TA treatment on macrophage polarization, both RAW 264.7 and THP-1 cells were pre-treated with TA for 1 h. Following the removal of TA treatment, cells were washed with sterile phosphate buffered saline (PBS) and then stimulated with LPS. Subsequently, A549 cells were cultured with macrophage-derived conditioned medium for 36 h to analyse EMT.

Determination of morphological analysis

At the end of the experimental period, the cells were photographed (Nikon Eclipse Ti) and taken for morphological analysis. Morphological changes of the cells were quantitatively determined by calculating cell circularity using ImageJ software as described previously [19]. A value of 1.0 indicates a perfect circle and cell circularity value decreases when there is an alteration in the morphology of A549 cells from cobblestone shape to elongated shape.

Real-time quantitative PCR (qRT-PCR) analysis

Total RNA was extracted from both macrophages and epithelial cells using TRIzol reagent, reverse transcribed, and subjected to qRT-PCR analysis. The expression levels of human endogenous genes such as ZO-1 (Zonula occludens-1) (sense, AGAAGGATGTTTATCGTCGCATT; antisense, CCAAGAGCCCAGTTTTCCAT), CK19 (Cytokeratin-19) (sense, CATGAAAGCTGCCTTGGAAGA; antisense, TGATTCTGCCGCTCACTATCA), CLDN (sense, CAATGCCAGGTACGAATTTGG; antisense, TGGATAGGGCCTTGGTGTTG), N-CAD (sense, TGTTTGACTATGAAGGCAGTGG; antisense, TCAGTCATCACCTCCACCAT), VIM (sense, TGTCCAAATCGATGTGGATGTTTC; antisense, TTGTACCATTCTTCTGCCTCCTG), COL1 (Type-1-collagen) (sense, CAGCCGCTTCACCTACAGC; antisense, TTTTGTATTCAATCACTGTCTTGCC), and GAPDH (Glyceraldehyde 3-phosphate dehydrogenase) (sense, CTCCTCTGACTTCAACAGCGACA; antisense, GAGGGTCTCTCTCTTCCTCTTG) were quantified using fluorogenic SYBR green and detection system. In RAW 264.7 cells, gene expression was performed using mouse-specific primers as follows: Cd32 (Fc fragment of IgG, low affinity IIb, receptor) (sense, AATCCTGCCGTTCCTACTGATC; antisense, GTGTCACCGTGTCTTCCTTGAG), iNos (Inducible nitric oxide synthase) (sense, CCCTTCAATGGTTGGTACATGG; antisense, ACATTGATCTCCGTGACAGCC), Il-1β (sense, CAACCAACAAGTGATATTCTCCATG; antisense, GATCCACACTCTCCAGCTGCA), Mcp-1 (Monocyte chemoattractant protein-1) (sense, CAGGTCCCTGTCATGCTTCT; antisense, GTGGGGCGTTAACTGCATCT), Mip-1α (Macrophage inflammatory protein-1 alpha) (sense, TCTGCGCTGACTCCAAAGAG; antisense, GTGGCTACTTGGCAGCAAAC), Tlr4 (sense, CCTGTAGAGATGAATACCTC; antisense, TGTGGAAGCCTTCCTGGATG), and Gapdh (sense, TGCACCACCAACTGCTTAG; antisense, GGATGCAGGGATGATGTTC). The absolute expression value for each gene was normalized to that of endogenous control, and the values of vehicle-treated samples were set as 1. The number of samples used in each experimental condition is indicated in the figure legends.

Detection of cytokine production

Cytokines such as Tnf-α (Tumor necrosis factor-alpha), Ifn-γ, Il-1β, Il-2, Il-6, and Il-12 levels in cell-free culture supernatants were quantified using the sandwich-ELISA kit, according to the manufacturer's instructions.

Nitric oxide (Griess) assay

The iNos activity was assessed by measuring the levels of nitrite, a stable break down product of nitric oxide metabolism, in cell culture supernatants. Briefly, supernatants were combined with an equal volume of 2% sulphanilamide (Sigma) and 0.1% N-1-naphthylethylenediamine dihydrochloride and incubated at room temperature for 30 min, then the absorbance was measured at 540 nm using a microplate reader. Nitrite levels were expressed as a percentage of increase or decrease over their respective controls.

Western blot analysis

Cells were lysed in RIPA lysis buffer and the protein concentration were measured using the Bradford protein assay kit. Equal amount of extracts was separated by 12% sodium dodecyl sulfate-polyacrylamide gel electrophoresis (SDS-PAGE) and transferred onto polyvinylidene difluoride (PVDF) membrane. The membranes were incubated with specific primary antibodies at 4 °C overnight, followed by incubation with appropriate secondary antibodies. The blots were visualized with ECL detection reagent. Tubulin was used as an internal control for the total protein. Bands were quantified by densitometry using ImageJ software. Further,

the phosphorylated form of the protein was normalized against its respective total protein.

Immunoprecipitation

RAW 264.7 cells were pre-treated with TA (20 µM) or vehicle for 1 h, washed to remove TA, and then incubated with LPS (1 µg/mL) for an additional 20 min. Cells were lysed with RIPA lysis buffer and the protein concentration was measured using the Bradford protein assay kit. Equal amount of protein from cell lysates was separated by 12% SDS-PAGE and transferred to PVDF membrane. For immunoprecipitation, 500 µg of protein was incubated with 2 µg of MD2 antibody and gently rotated at 4 °C for overnight. The immunocomplexes were collected with protein A/G plus-agarose beads. After washing three times with ice-cold PBS, the immunoprecipitated protein was solubilized with Laemmli sample buffer. The solubilized proteins were analysed through Western blotting with anti-TLR4 antibody.

Flow cytometric analysis to detect surface TLR4 expression

Raw 264.7 cells were pre-treated with TA for 1 h and then exposed to LPS for an additional 1 h. At the end of 1 h, cells were harvested, washed, and stained with BV (Brilliant violet) 421-labeled anti-TLR4 antibody for 30 min. Then, stained cells were washed with cold PBS and fixed with 1.5% paraformaldehyde. The staining of the surface TLR4 was analysed with a flow cytometer (BD FACSCanto II, San Jose, CA). A total of at least 50,000 events was acquired and analysed. Mean Fluorescent Intensity (MFI) for the fluorescence against TLR4 was measured with the acquired cells for comparative analysis within different experimental groups with the help of FlowJo software (Treestar, FlowJo, LLC).

The effect of TA on LPS-FITC binding to macrophages using flow cytometry

Raw 264.7 cells (10^6 cells) were incubated for 1 h at 37 °C with TA (20 µM) in DMEM supplemented with 10% FBS. Pre-incubated cells were washed with PBS, then incubated with LPS-FITC (10 µg/mL) for another 15 min and then washed again. After washing, the binding of LPS-FITC to cells was analysed by flow cytometry. A total of at least 10,000 events was acquired and analysed. MFI for FITC was measured with the acquired cells for comparative analysis within different experimental groups with the help of FlowJo software (Treestar, FlowJo, LLC).

In silico analysis

To understand the binding mechanism of the TA, a crystal structure of the TLR4-MD2 complex (PDB ID: 5IJC) was retrieved and binding potency was analysed independently [20]. The tertiary structure of the protein was prepared and furthermore missing side chains, loops, and hydrogens were added using the Protein preparation wizard, Maestro, Schrodinger 2017-4 [21]. The co-crystallized structure has various co-factors and molecules, which were verified and unreactive molecules were removed before proceeding to the molecular docking analysis [22]. The protein was subjected to H-bond optimization and energy minimization using an OPLS-3 force field. The prepared protein was subjected to a receptor grid generation panel of Maestro, Schrodinger 2017-4 for the grid generation. The active site was defined and the grid box was generated around the binding site pocket of the TLR4. The active site residues of TLR4 are Asn129, Lys153, Ser206, Phe262, Asp264, Arg256, Arg288, Met311, Ser332, and Asp377 [23], further three more hydrophobic residues (Phe440, Leu444, and Phe463) responsible for MD2 conjugation were also included [24]. The ligand preparation of TA was performed [13] and the prepared TA was allowed to dock on the binding site of the TLR4-MD2 complex through Glide XP mode using Glide, Maestro, Schrodinger 2017-4. The results were analysed for the binding scores, interactions, affinity and binding conformation of the TA. The TA compound was docked in the TLR4 and MD2 protein receptor as a competitive binding to determine the binding behavior of the TA compound in their receptor.

FTIR (fourier transform infrared spectroscopy) analysis

First, recombinant TLR4 (100 ng) was pre-mixed with TA (20 µM) for 1 h at 4 °C. FTIR spectra were recorded for the TA, TLR4, and TA-TLR4 complex. FTIR studies have been performed using a spectrum instrument PerkinElmer, Spectrum RX I, Waltham, MA, with the diffuse reflectance mode at a resolution of 4 cm^{-1} in the range of 400–4000 cm^{-1}.

HPLC (high performance liquid chromatography) analysis

For complex preparation, recombinant TLR4 protein (100 ng/0.5 mL) was pre-incubated with an equal volume of solution containing TA (20 µM) for 1 h at 4 °C with a little shaking, and then the solution was centrifuged at 4000 rpm for 15 min with centrifugal filters (5 kDa membrane; GE Healthcare, Chicago, IL, USA). The filters could prevent TLR4 or TA-binding TLR4 flowing into the filtrate. Similarly, pure TA without centrifugal ultrafiltration and TA subjected to centrifugal ultrafiltration were also taken for the

analysis. RP-HPLC analysis was carried out for the resultant filtrate using Agilent 1220 Infinity LC II system (Agilent Technologies, Ratingen, Germany) incorporated with phenomenex silica C-18 (250 × 4.6 mm, 5 µm) column. The filtrate (20 µl) was injected into the column and eluted with gradient mobile phase composition of 0.1% TFA (Trifluoroacetic acid) (V/V) in water as mobile phase A, 100% methanol has been used as a mobile phase B (0th min A:90%, B:10%; 5th min A:80%, B:20%; 10th min A:60%, B:40%, 15th min A:90%, B:10%), and the absorbance was recorded as chromatogram at 280 nm for 15 min at a flow rate of 1 mL/min.

Statistical analysis

Results were expressed as mean ± SD. Statistical analysis was performed non-parametrically using the Kruskal–Wallis test to determine significant differences between various experimental groups. $P \leq 0.05$ was considered statistically significant.

Results

TA inhibits polarized macrophage-induced EMT in epithelial cells

We first cultured A549 cells for 36 h with CM from polarized RAW 264.7 cells and analysed for morphological changes. We found that A549 cells exhibited morphological changes, where epithelial cells lose their cobblestone morphology and gained elongated shape or fibroblast-like appearance, a hallmark of EMT (Fig. 1a). These morphological changes were quantitatively determined by the circularity of the cells (Fig. 1b). By contrast, CM from polarized macrophages that pre-treated with TA did not alter the morphology of A549 cells. Along with these morphological alterations, the gene expression of epithelial (ZO-1, CK19, and CLDN) and mesenchymal markers (N-CAD, VIM, and COL1) was analysed in A549 cells (Fig. 2). On M1-CM treatment of A549 cells, epithelial-specific markers such as *ZO-1*, and *CK-19* decreased significantly, while the expression of *CLDN* was significantly up-regulated (Fig. 2a). As expected, M1-CM significantly induced mesenchymal markers (*N-CAD*, *VIM*, and *COL1*) expression in A549 cells (Fig. 2b). More importantly, after treatment with TA, the supernatant from polarized macrophages did not induce the expression of mesenchymal markers in A549 cells.

Consistent with the mRNA changes, M1-CM decreased protein expression of epithelial marker E-CAD, while it increased CLDN expression compared to CM from control cells. Conversely, the expression of mesenchymal markers such as N-CAD and VIM was enhanced by the addition of the M1-CM. These effects were effectively reversed when polarized macrophages were pre-treated with higher dose of TA (20 µM) (Fig. 2c). Next, we examined whether M1-CM from THP-1 cells induced alterations of EMT markers in

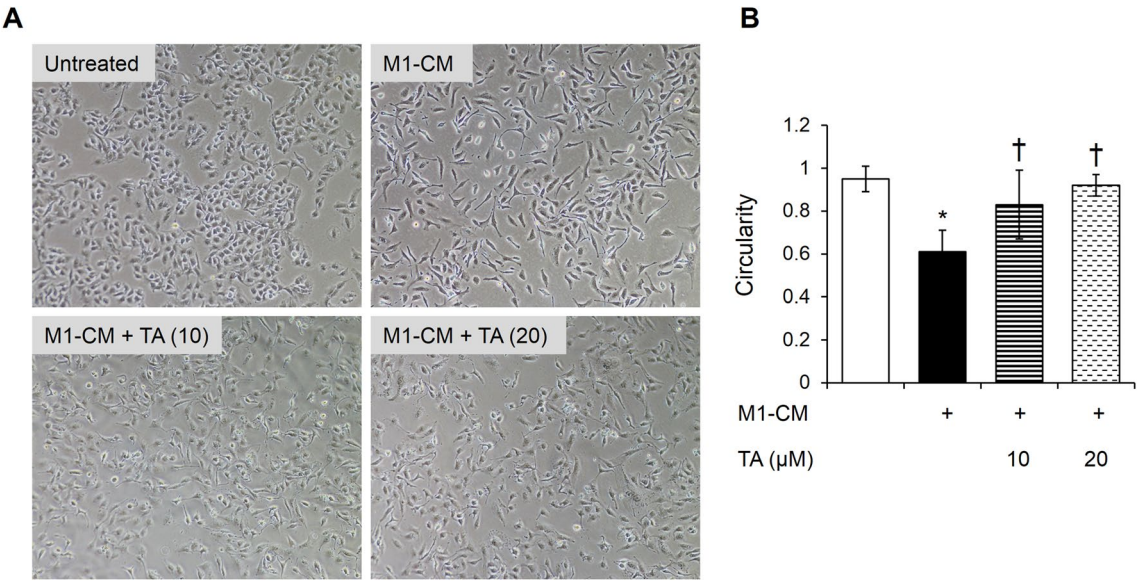

Fig. 1 TA pre-treated M1 macrophage conditioned-medium could not promote EMT in A549 cells. RAW 264.7 cells were pre-treated with TA (10 or 20 µM) for 1 h, washed twice to remove TA, and stimulated with LPS (100 ng/mL) for 24 h in serum-free medium to generate M1 macrophages. Then, A549 cells were cultured with the supernatant of polarized macrophages for 36 h. After culturing, cells were photographed and cell morphology was evaluated. **a** Representative images of the morphology of A549 cells cultured with macrophage-conditioned medium (Magnification, × 10). **b** Cell circularity was calculated using ImageJ software. Data are expressed as mean ± SD ($n = 4$). $^{*}P \leq 0.05$ vs. normal medium, $^{\dagger}P \leq 0.05$ vs. M1-CM

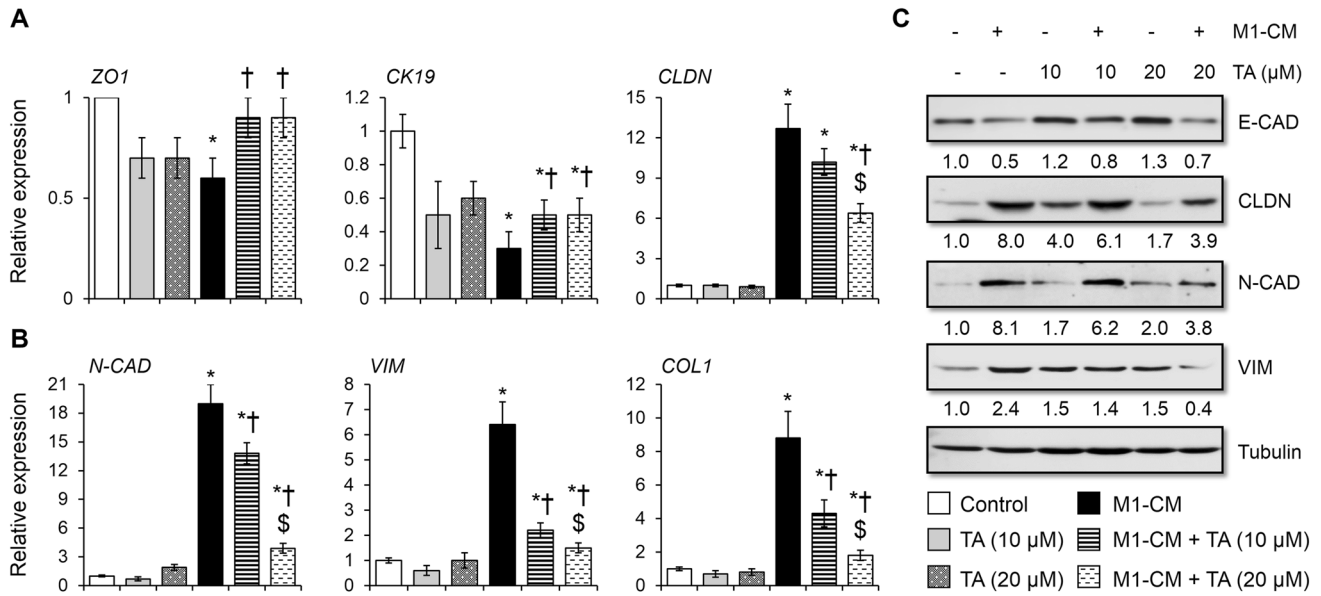

Fig. 2 TA inhibits polarized macrophage-induced EMT-related gene and protein expression in A549 cells. RAW 264.7 cells polarization and conditioned-medium incubation were done as described above. The mRNA expression of epithelial **a** and mesenchymal **b** markers was measured by qRT-PCR. The value of control was considered as one unit. Data are expressed as mean ± SD ($n = 3$). **c** Immunoblot results show the expression levels of epithelial and mesenchymal markers after 36 h in cell culture. The band intensity was quantified using tubulin as an internal control, and the value of control was considered as one unit. $^{*}P \leq 0.05$ vs. normal medium, $^{\dagger}P \leq 0.05$ vs. M1-CM. $^{\$}P \leq 0.05$ vs. TA (10 μM) + M1-CM group

A549 cells. As shown in Fig. S1, compared with native, M1-CM induced mesenchymal markers expression at both mRNA and protein levels. However, TA pre-treated CM prevented EMT. Overall, our data suggest that TA pre-treatment dose-dependently suppresses epithelial cells from transitioning to a mesenchymal-like phenotype that was induced by polarized macrophages.

Inhibitors of ERK1/2 and p38 reduced M1-CM induced EMT in A549 cells

Next, we examined the M1-CM mediated signaling cascade activation in A549 cells by incubating the cells at different time points (0–300 min). M1-CM predominantly activated ERK1/2 and p38 MAPK, phosphorylation peaking at 15, 90, 150, and 180 min, as shown by Western blotting analysis (Fig. 3a). We also examined whether TA pre-treated M1-CM blocked ERK1/2 and p38 MAPK phosphorylation in A549 cells upon incubation. It was apparent that TA pre-treated M1-CM inhibited the phosphorylation of all these molecules at 15 min (Fig. 3b). We then investigated whether ERK1/2 and p38 MAPK activation induced by M1-CM was responsible for EMT in A549 cells. We pre-treated A549 cells with inhibitors of ERK1/2 (PD98059) and p38 (SB203580), followed by incubation with M1-CM. As shown in Fig. 3c, inhibitor of ERK1/2 or p38 alone is not sufficient to effectively block M1-CM induced mesenchymal markers (N-CAD and VIM) expression. However, the combination of both inhibitors had a more pronounced effect in controlling mesenchymal markers expression than either single agent, indicating that blocking of both ERK and p38 MAPK activation is necessary to inhibit M1-CM induced EMT in A549 cells.

TA inhibits LPS-induced M1 polarization and cytokine production in RAW 264.7 cells

To further identify the influence of TA on macrophage polarization and on the release of EMT-related cytokines, we analysed mRNA expression and secretome profile for cytokines. As shown in Fig. 4a, macrophages of the M1 phenotype expressed significantly higher mRNA levels of M1 markers such as Cd32, iNos, Il-1β, Mcp-1, and Mip-1α compared to M0 macrophages. Compared with LPS-treated cells, TA markedly inhibited the mRNA expression of these markers (Fig. 4a). Consistent with mRNA result, the activity of iNos was significantly higher in the supernatant of LPS-treated cells (Fig. 4b). Further, we analysed secretome profile of EMT-related cytokines by M1 macrophages those were pre-treated with or without TA. Results demonstrated that M1 macrophages significantly released higher levels of cytokines such as Tnf-α, Ifn-γ, Il-1β, Il-6, and Il-12 in the supernatant compared to M0 macrophages (Fig. 4c) as

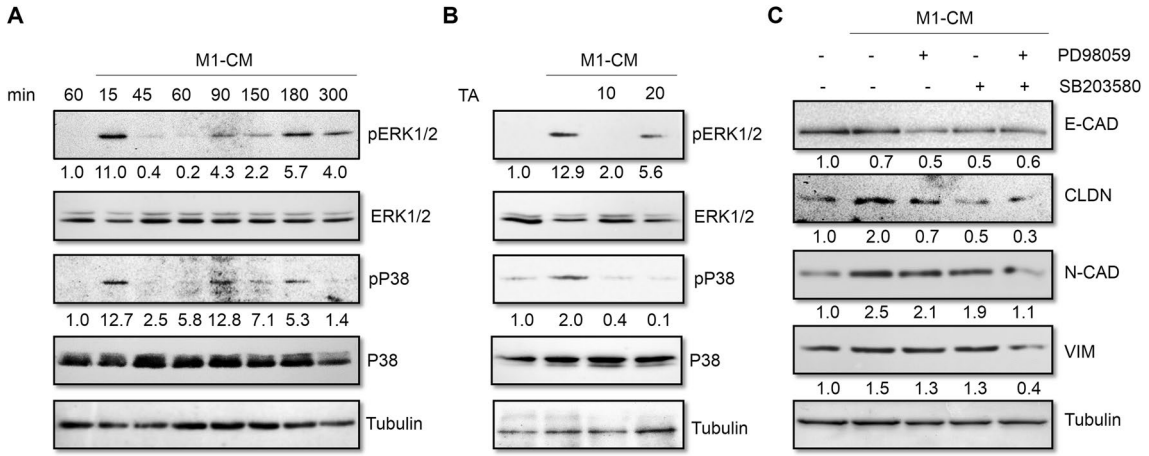

Fig. 3 Activation of MAPK (ERK and p38) is required for M1-CM induced EMT in A549 cells. Overnight serum-starved cells were incubated with CM from different experimental groups. **a** Representative western blot analysis shows the phosphorylation of ERK1/2 and p38 MAPK in A549 cells following incubation with M1-CM at different time points. **b** Western blot analysis shows the phosphorylation of ERK1/2 and p38 MAPK in A549 cells at 15 min following incubation with TA pre-treated M1-CM. **c** Immunoblotting results show the effect of ERK and P38 inhibitors on the expression of mesenchymal markers in A549 cells at 36 h following incubation with M1-CM. The band intensity was quantified using tubulin as an internal control, and the value of control was considered as one unit. The phosphorylated form of proteins was normalized against their respective total protein

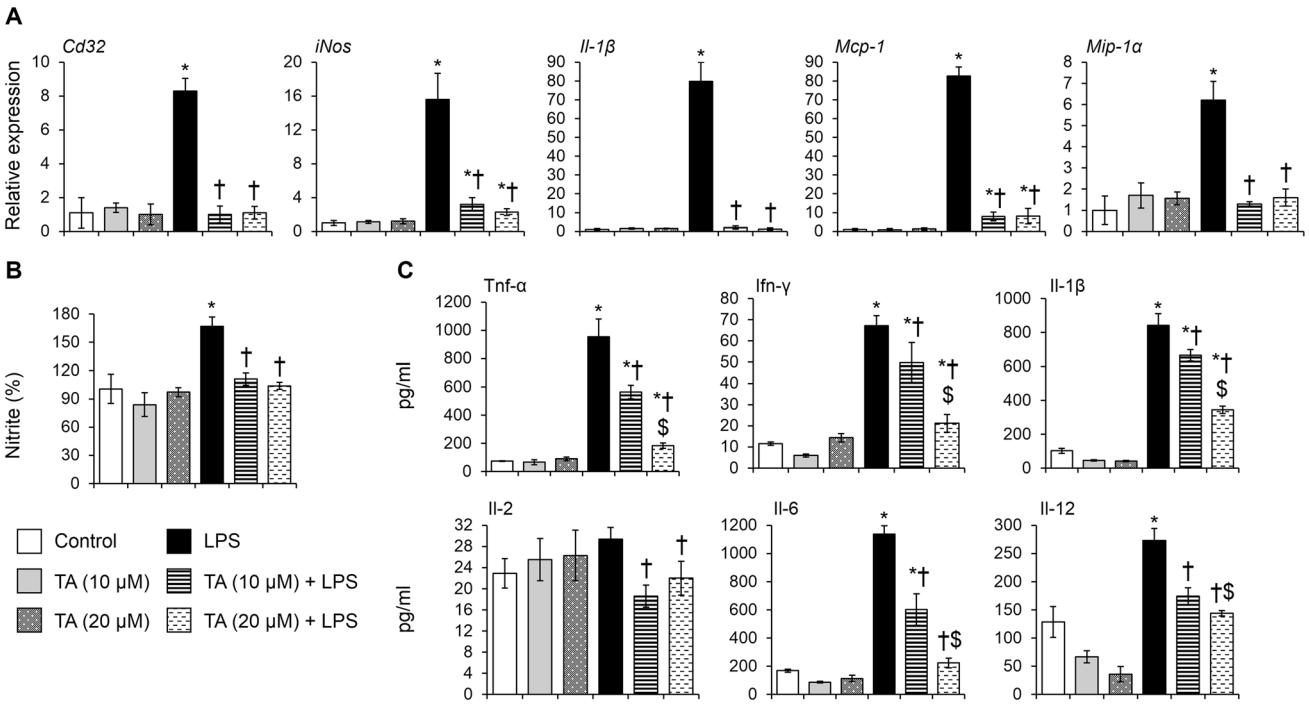

Fig. 4 TA prevents LPS-induced macrophage polarization and the production of cytokines/chemokines in RAW 264.7 cells. TA pre-treatment and macrophage polarization were done as described above. **a** The mRNA expression of Cd32, iNos, Il-1β, Mcp-1, Mip-1α, and Gapdh was determined 6 h following LPS treatment by qRT-PCR analysis. The value of control was considered as one unit. **b** The iNos activity in the cell culture supernatant was determined by measuring the nitrite levels. **c** The secretory levels of M1 markers in the culture supernatant at 24 h following LPS treatment as quantified by sandwich-ELISA method. Data are expressed as mean ± SD ($n = 3$). $^{*}P \leq 0.05$ vs. control, $^{\dagger}P \leq 0.05$ vs. LPS-treated cells, $^{\$}P \leq 0.05$ vs. TA (10 μM) + LPS group

determined by ELISA. Of these cytokines, no significant difference in the level of Il-2 was observed between the M1 and M0 phenotypes. Interestingly, TA pre-treatment inhibited macrophage polarization and the secretion of these cytokines in the dose-dependent manner.

TA negatively regulates LPS-induced activation of MAPKs and NF-kB and the expression of TLR4 in RAW 264.7 cells

We first determined the effects of TA on LPS-activated downstream signaling in the TLR4/MD2 cascade mainly MAPKs and NF-kB. Figure 5a shows that Erk1/2, p38, and NF-kB phosphorylation occurred at 45 min and the levels reached the peak at 90 min following LPS treatment. However, pre-treatment with TA for 1 h, followed by treatment with LPS for 90 min decreased the phosphorylation of all these molecules (Fig. 5b). Given that TA attenuated LPS-induced activation of both MAPK and NF-kB, it was of interest to identify whether TA affects the expression of Tlr4, the main upstream sensor of LPS, which plays a central role in activating various signaling pathways including MAPKs. As shown in Fig. 5c, the mRNA expression of Tlr4 was increased significantly in 1 h LPS-treated cells compared to vehicle- and TA alone-treated cells. However, TA pre-treatment significantly prevented LPS-induced *Tlr4* expression. We further studied the effect of TA on the surface expression of Tlr4 by flow cytometry (Fig. 5d). While there was an increase in the surface expression of Tlr4 in LPS-treated cells, pre-treatment with TA dampened Tlr4 surface expression. Taken together, these results indicated that TA suppresses LPS-mediated effect through down-regulating TLR4 expression and activation of MAPKs and NF-kB signaling.

TA inhibits LPS binding to TLR4/MD2

In RAW 264.7 cells, we first investigated if TA is able to reduce LPS binding to cell surface. Accordingly, cells were incubated with LPS-FITC in the presence or absence of TA. Untreated cells served as a negative control. The results, shown in Fig. 6a, revealed that LPS-FITC treated cells showed significantly increased MFI compared with control (non LPS-FITC treatment), however, TA pre-incubation showed markedly lower fluorescence compared to LPS-FITC treated cells, suggesting that LPS binding with RAW 264.7 cells was effectively inhibited by TA. Further, upon binding with a hydrophobic pocket of MD2, LPS triggering the increased formation of receptor multimer composed of two sets of TLR4/MD2/LPS, leading to the activation of intracellular signals. Hence, we next examined whether TA interferes with interactions between LPS and TLR4/MD2 by immunoprecipitation assay. As shown in Fig. 6b, LPS profoundly increased TLR4/MD2 complex formation, whereas pre-treatment with TA reduced the amount of MD2 bound to

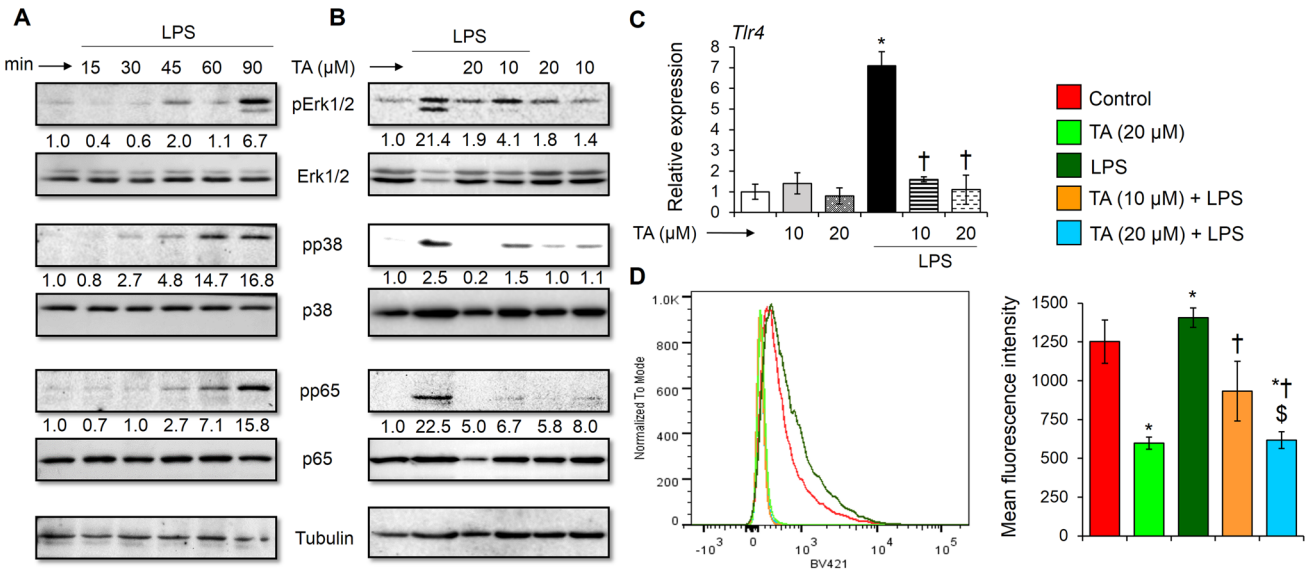

Fig. 5 TA treatment dampened LPS-induced activation of MAPK (ERK and p38), NF-kB, and TLR4 expression in RAW 264.7 cells. Following overnight serum starvation, cells were pre-incubated with TA (10 or 20 μM) for 1 h, washed twice to remove TA, and stimulated with LPS (100 ng/mL) in serum-free medium at indicated time points. **a** Representative western blot analysis shows the phosphorylation of Erk1/2, p38, and NF-kB in RAW 264.7 cells after treatment with LPS. **b** Immunoblot results show the phosphorylation of Erk1/2, p38, and NF-kB in RAW 264.7 cells at 90 min following TA and LPS treatment. The mRNA (**c**) and surface (**d**) expression of Tlr4 in cells following 1 h LPS treatment based on qRT-PCR and flow cytometry analysis, respectively. Bar graph (right side) represents the mean fluorescence intensity. Data are expressed as mean ± SD ($n = 3$–4). $^{*}P \leq 0.05$ vs. control, $^{\dagger}P \leq 0.05$ vs. LPS-treated cells, $^{\$}P \leq 0.05$ vs. TA (10 μM) + LPS group

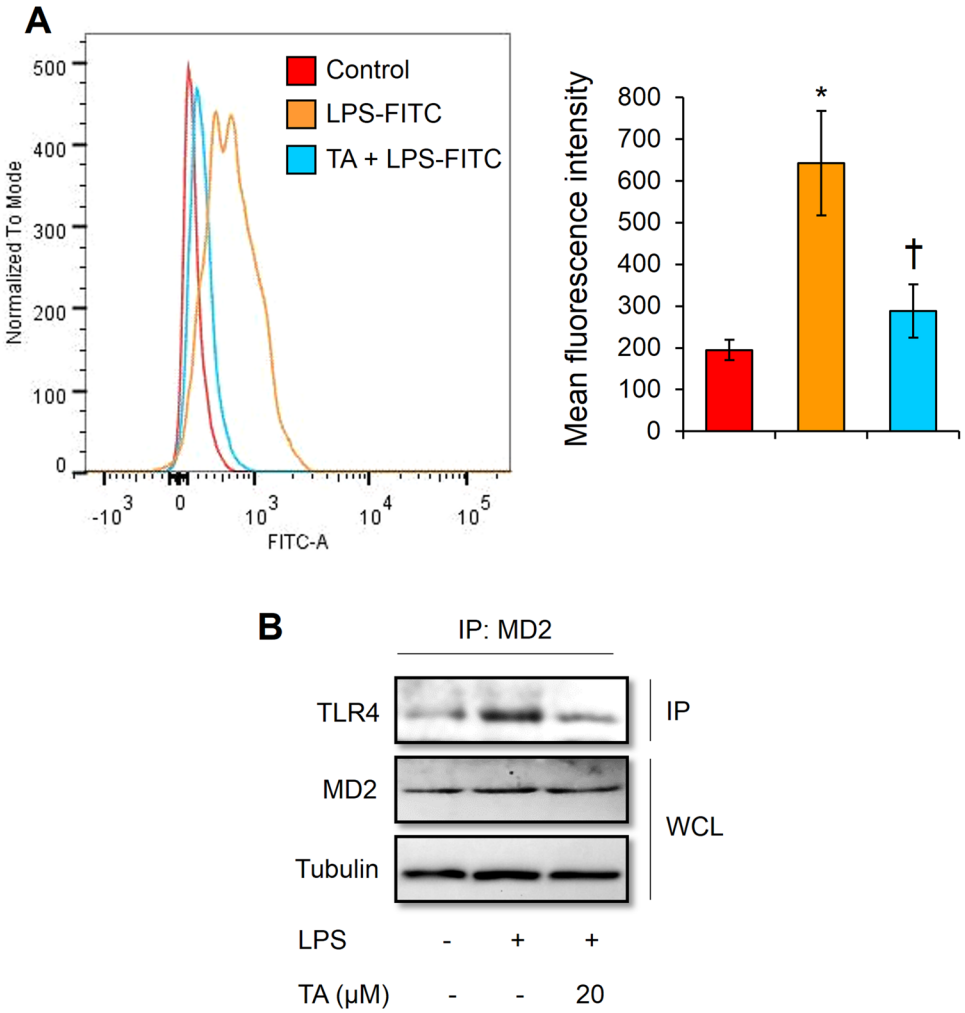

Fig. 6 The antagonistic effect of TA on the binding of LPS to TLR4/MD2 in RAW 264.7 cells. Cells were pre-incubated with TA (20 μM) for 1 h, washed to remove TA, and then incubated with LPS-FITC (10 μg/mL) for an additional 15 min. **a** The cells were washed, and the binding of LPS-FITC was analysed by flow cytometry. The bar graph (right side) represents the mean fluorescent intensity of FITC within different experimental groups. The background was taken using untreated macrophages (red line). **b** Immunoprecipitation assay shows that TA pre-treatment (20 μM) reduced the formation of TLR4/MD2 complex induced by LPS (1 μg/mL). Data are expressed as mean ± SD ($n = 3$). $^{*}P \leq 0.05$ vs. control, $^{\dagger}P \leq 0.05$ vs. LPS-FITC treated cells (Color figure online)

TLR4. These results further demonstrate that TA interferes with the interaction of LPS with TLR4/MD2.

Binding analysis of TA in TLR4

To further identify whether TA could interact with TLR4 and thereby preventing LPS-mediated activation of TLR4 signaling pathways, we performed molecular docking, FTIR, and HPLC analyses. The molecular docking results provided a significant result to underline the TA binding mechanism in TLR4 and MD2 complex (Fig. 7). To examine the binding ability of TA in MD2 alone, separate docking analysis was done. But, TA was not able to dock in the receptor due to the tiny cavity of the molecule. However, TA was observed to have better docking score with TLR4 than MD2. The glide XP score and glide energy score of TA in TLR4 were -18.113 kcal/mol and -110.885 kcal/mol, respectively (Fig. 7). TA binding also disrupts the non-covalent interactions between TLR4 and MD2. Most specifically, the hydrophobic interactions such as Phe440, Leu444, and Phe463 were disappeared after TA binding. Therefore, the docking studies revealed that the TLR4 acts as a best receptor to bind with TA. The hydrogen bond interactions observed between the TA and TLR4 are Ser206, Glu229, Arg256, Arg288, Arg380 and Asp403. In addition, the residues Arg256 and Arg380 have formed pi–pi and pi-cation interactions with TA. Further, TA has also formed hydrogen bonds with MD2 residues like Tyr73 and Asp100, when it was complexed with TLR4.

Figure 8a shows the FTIR spectrum to identify the interaction of TA with TLR4. The broad peaks in the region of 3000–3500 cm^{-1} were assigned to –OH stretching for the hydrogen bond with the physical adsorbed water molecules. TA exhibits a characteristic peak at 1637 cm^{-1}, which is associated with C=C stretching of the benzene ring [25]. Similarly, the TLR4 spectrum shows the characteristic peaks at 1638 and 1694 cm^{-1} is associated with C=O stretching [26]. Furthermore, the band at 1637 cm^{-1} (C=C stretching) in TA is shifted to 1639 cm^{-1} after the incubation of TA with TLR4. Another important observation is that after TLR4 incubated with TA, the absorption related to the C=O

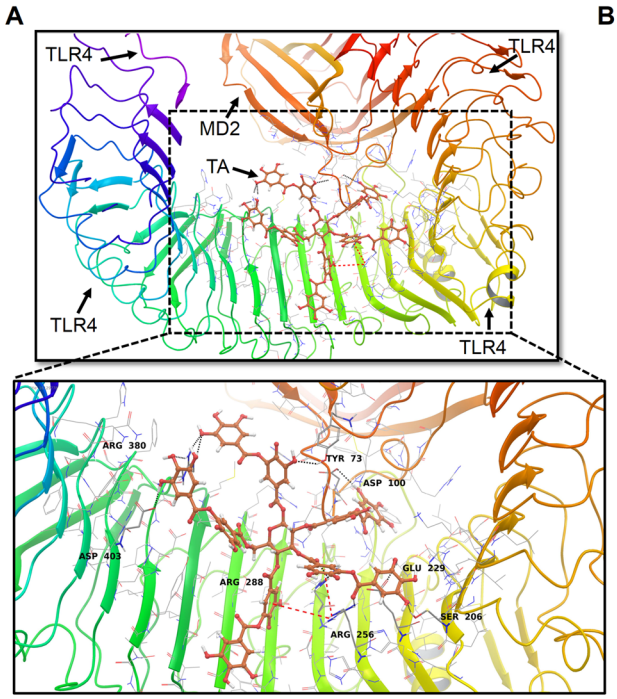

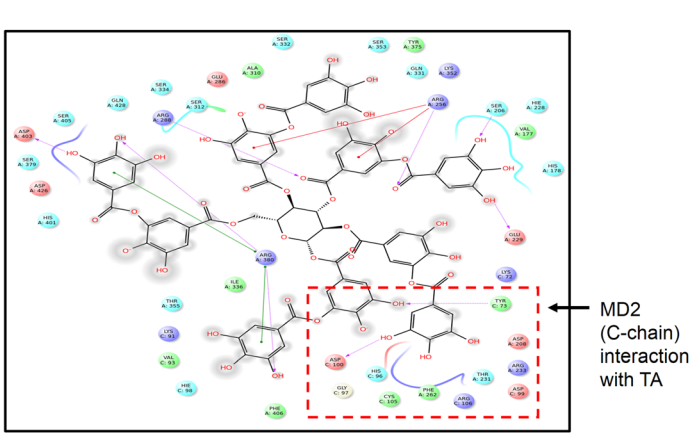

C

S. No.	Protein	Glide XP score (kcal/mol)	Glide Energy (kcal/mol)	Interacting residues
1	TLR4	-18.113	-110.885	Ser206, Glu229, **Arg256**, Arg288, **Arg380**, Asp403
2	MD2	*	*	*

Fig. 7 In silico analysis of TA interaction with TLR4/MD2 complex. **a** 3-D image showing the interaction of TA in the active sites of TLR4/MD2 complex. **b** 2-D interaction image of the TA with TLR4/MD2. **c** Calculated binding energy and interacting residues of TLR4 with docked complex. *MD2 has an unfavorable binding cavity to accommodate TA into its active site. TA is a big molecule, hence it requires a large hydrophobic area in the receptor molecule. Bolded residues were having hydrogen bonds as well as pi–pi and pi-cation interactions with TA

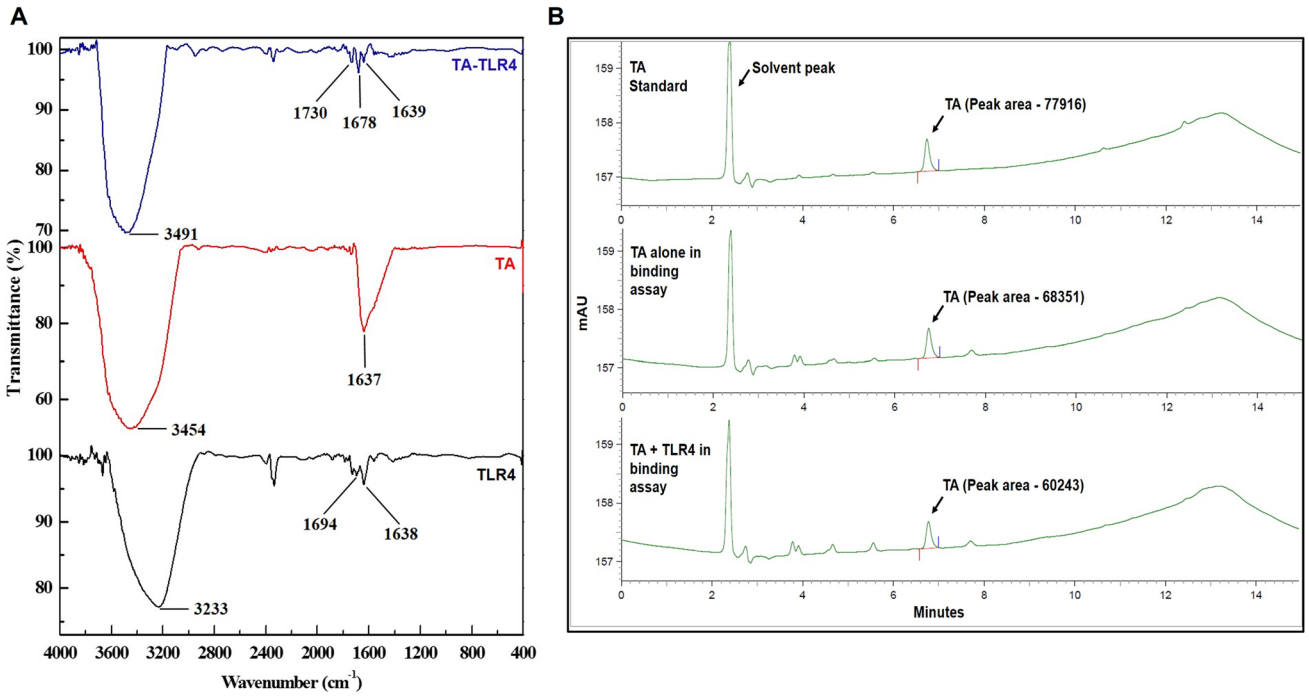

Fig. 8 Analysis of binding of TA to TLR4. **a** FTIR spectra and **b** HPLC analysis to show the binding of TA with TLR4

stretching (1638 and 1694 cm^{-1}) of the TLR4 clearly shifts to longer wavenumbers (1678 and 1730 cm^{-1}).

Furthermore, by comparing the HPLC results (Fig. 8b), we found that TA peak area (as identified by HPLC in filtrate) from TA-TLR4 group became lower (60243) than the peak areas of TA with centrifugal ultrafiltration (68351) and TA without centrifugal ultrafiltration (77916), indicating a loss of TA after incubation with TLR4. Altogether, our results suggest that there might be a possible interaction between TA and TLR4.

Discussion

In many chronic inflammatory diseases, fibrosis is the final pathological state and may lead to organ dysfunction. Macrophages are considered to be crucial determinants of fibrosis development and resolution as they are extremely plastic in response to microenvironmental signals. According to the microenvironment stimuli, both resident and infiltrating macrophages can acquire distinct phenotypes and biological functions. They may be considered as M1 and M2 macrophages. However, there is a strong evidence that both inflammatory and regulatory macrophages may participate in the pro-fibrotic processes [9, 27–29]. In the context of fibrosis, EMT begins as a pro-fibrogenic event that generates mesenchymal cells (myofibroblast) to reconstruct tissues following inflammatory injury. However, in the case of chronic inflammation, EMT continues to respond to ongoing inflammation, finally leading to deterioration of tissue architecture [5, 6]. There are different ways by which M1 macrophages promote EMT. First, macrophages induce EMT when they directly contacted with epithelial cells [30]. Second, they generate cytokines/chemokines that activate EMT, either by production of pro-inflammatory cytokines such as TNF-α and IL-1β, or chemokine, such as MCP-1 [31]. In this study, we used in vitro experiments to demonstrate that the CM from polarized macrophages could induce EMT in lung epithelial cells. However, this effect was not observed with the supernatant from polarized macrophages that were pre-treated with TA. Our results further demonstrated that TA blocked LPS-induced macrophage polarization possibly through interacting with TLR4.

During the process of EMT, diminished expression of various epithelial markers (E-CAD, occludins, and cytokeratins) and the enhanced expression mesenchymal markers [N-CAD, VIM, and FN (Fibronectin)] are associated with the epithelial cells [5, 6]. EMT converts adherent epithelial cells to motile mesenchymal cells with increased capacity of ECM components production, which plays an important role in both experimental and clinical lung fibrosis [6]. A large number of studies confirmed the importance of EMT in repair and scar formation following epithelial injury during pulmonary fibrosis. For instance, Yamada et al. provided histological evidence for EMT in patients with pulmonary fibrosis and non-specific interstitial pneumonia [32]. Similarly, epithelial cells isolated from IPF lungs are reported to express high levels of mesenchymal markers [33]. Recently, regulatory network analysis revealed that the EMT pathway was significantly enriched with the differentially expressed IPF (Idiopathic Pulmonary Fibrosis) genes [34]. In experimental lung fibrosis, it has been proved that 33% of the mesenchymal population during lung fibrosis was derived from epithelial origin [35]. Further, the tight junction protein CLDN is believed to be important for the maintenance of epithelial barrier function and thus, the expression is reported to decrease during EMT [36]. However, our results showed that CLDN expression is increased upon incubation with M1-CM in A549 cells. This result is consistent with others report showing that CLDN expression is enhanced in response to pro-inflammatory cytokine to induce fibroblast-like morphology and enhance cell migration in A549 cells [37, 38]. Overall, our data suggested that TA pre-treatment attenuated M1 macrophage-mediated EMT in lung epithelial cells.

Recent studies have shown that the inflammatory mediators (cytokines/chemokines), particularly those released by M1 macrophages promote EMT. Among the cytokines, TNF-α, IFN-γ, IL-1β, IL-6, and MCP-1 have been previously reported as potent inducers of EMT in epithelial cells through various signaling pathways. For instance, TNF-α is reported to exhibit mesenchymal responses through the activation of ERK and p38 MAPK in endometriotic epithelial cells [39]. Further, IL-6 promotes EMT in human peritoneal mesothelial and in A549 cells through JAK2/STAT3 (Janus kinase 2/Signal Transducer and Activator of Transcription 3) and ERK signaling pathways, respectively [40, 41]. MCP-1 is considered as a contributory factor for EMT in MCF-7 cells by down-regulating E-CAD expression and up-regulating mesenchymal markers expression [42]. MCP-1 also increased the expression and nuclear accumulation of SNAIL to mediate EMT associated cell proliferation and migration through activating ERK signaling and inactivating GSK-3β (Glycogen synthase kinase 3 beta) pathways. The authors further identified that inhibition of MEK/ERK by U0126 attenuated MCP-1-induced expression of mesenchymal markers and EMT. As many studies have demonstrated that MAPK is phosphorylated during cytokine-induced EMT, we pre-treated A549 cells with ERK and p38 MAPK inhibitors before incubation with M1-CM. The inhibitors reduced the effect of M1-CM induced EMT, indicating that activation of ERK and p38 MAPK is necessary for the EMT process.

Macrophages express Toll-like receptors (TLRs), which is more important for innate immunity. In particular, cytokine secretion occurs upon TLR4 activation by

LPS on these cells. Therefore, the expression levels of TLR4 determine the specificity of the signaling pathway activation and biological effects of LPS. In polarized macrophages, inhibition of TLR4 signaling was shown to reduce cytokines production and weakened their EMT inducing potential [43]. Hence, we further investigated the molecular mechanism by which TA modulates the LPS-induced macrophage polarization. In recent years, several non-lipid natural compounds have been reported to prevent LPS-induced pro-inflammatory signaling in multiple ways, such as targeting TLR4 directly, targeting LPS, binding directly to the MD2 pocket, and blocking the TLR4/MD2's recognition of LPS [44–49]. Therefore, we further investigated the interaction between TA and TLR4/MD2 at cellular and cell-free molecular levels. The results from in vitro LPS-FITC binding assay, immunoprecipitation, molecular docking studies, FTIR, and HPLC analyses revealed a possible interaction of TA with TLR4. Hence, we suggest that the suppressive effect of TA on LPS-induced inflammatory response may be dependent on the inhibition of LPS binding to TLR4 by TA. Nevertheless, it is also possible that TA may directly regulate the downstream of TLR4 signaling, which requires further investigation.

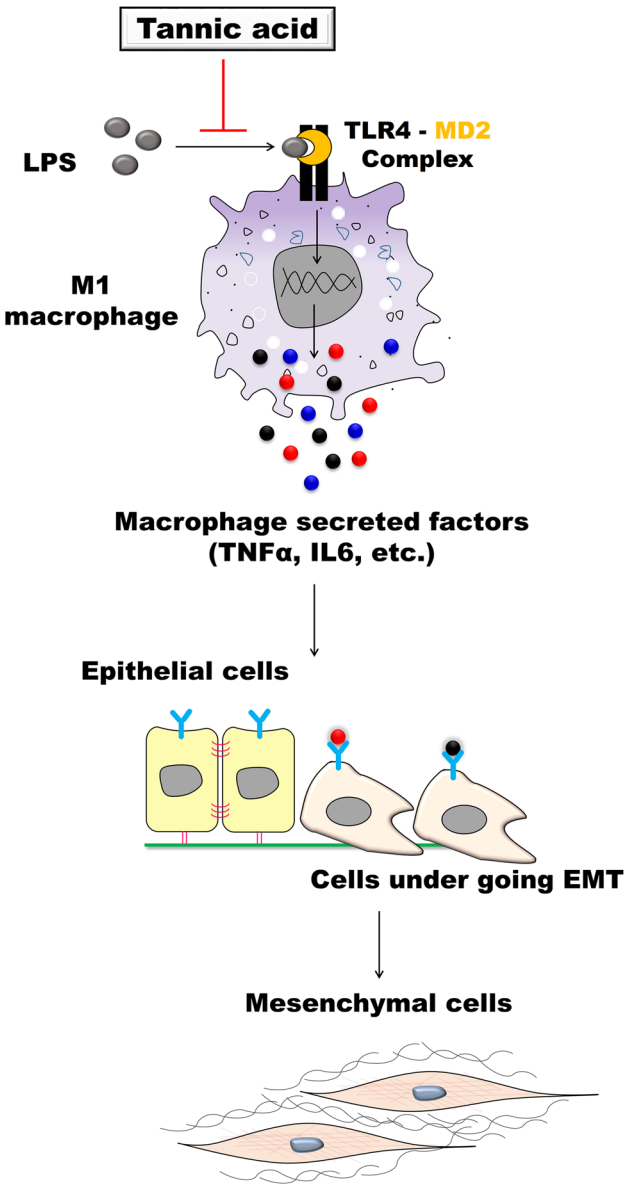

Fig. 9 Proposed model for the role of tannic acid in M1 macrophage-induced EMT. Tannic acid may directly interact with cell surface TLR4 in macrophages, thereby inhibiting LPS binding to TLR4, and subsequent activation of downstream signaling molecules. As a result, tannic acid impedes soluble factors secreted by M1 macrophages, which is responsible for promoting EMT in lung epithelial cells

In conclusion, we demonstrated that TA prevented M1 macrophage-induced EMT by inhibiting the macrophage polarization possibly through preventing the formation of LPS-TLR4/MD2 complex and blockage of subsequent downstream signaling activation (Fig. 9). These results provide new mechanistic bases for the therapeutic application of TA against chronic inflammatory diseases. However, future animal studies involving endotoxin-induced fibrosis model will be needed to elucidate this possibility.

Acknowledgements This work was supported by Ramalingaswami re-entry fellowship (BT/RLF/Re-entry/36/2013). S. R. is the recipient of Ramalingaswami re-entry fellowship from the Department of Biotechnology (DBT), Government of India. This study was also supported in part by the Department of Science and Technology (DST; Award No: YSS/2014/000125) (to S. R.), Government of India. The first author (A. S.) gratefully acknowledges the support of Indian Council of Medical Research (ICMR), New Delhi, India for the award of ICMR-Senior Research Fellowship (SRF; Award No: 45/03/2018-BMS/PHA/OL). The infrastructure of Department of Biotechnology, Anna University, BIT-campus is supported by the Department of Science and Technology-Fund for Improvement of S and T Infrastructure in Universities and Higher Educational Institutions (DST-FIST).

Author contributions SR has conceptualized, designed the experiments, acquired financial support, supervised the study, and wrote the manuscript; AS performed most of the experiments; DP and NR involved in the acquisition of data; AS, DP and SR analysed data and interpreted the results; AK and SKM participated in cytokine analysis; LL and KM participated in computational analysis; RB participated in flow cytometry analysis; RB, SKM and RP contributed reagents/materials/analysis tools.

Compliance with ethical standards

Conflict of interest The authors report no conflict of interest.

References

1. Gilbane AJ, Denton CP, Holmes AM. Scleroderma pathogenesis: a pivotal role for fibroblasts as effector cells. Arthritis Res Ther. 2013;15:215.

2. Ramming A, Dees C, Distler JH. From pathogenesis to therapy-Perspective on treatment strategies in fibrotic diseases. Pharmacol Res. 2015;100:93–100.
3. Willis BC, duBois RM, Borok Z. Epithelial origin of myofibroblasts during fibrosis in the lung. Proc Am Thorac Soc. 2006;3:377–82.
4. Iwano M, Plieth D, Danoff TM, Xue C, Okada H, Neilson EG. Evidence that fibroblasts derive from epithelium during tissue fibrosis. J Clin Invest. 2002;110:341–50.
5. Lamouille S, Xu J, Derynck R. Molecular mechanisms of epithelial-mesenchymal transition. Nat Rev Mol Cell Biol. 2014;15:178–96.
6. Stone RC, Pastar I, Ojeh N, Chen V, Liu S, Garzon KI, et al. Epithelial-mesenchymal transition in tissue repair and fibrosis. Cell Tissue Res. 2016;365:495–506.
7. Braga TT, Agudelo JS, Camara NO. Macrophages during the fibrotic process: M2 as friend and foe. Front Immunol. 2015;25:602.
8. Cao Q, Harris DC, Wang Y. Macrophages in kidney injury, inflammation, and fibrosis. Physiology (Bethesda). 2015;30:183–94.
9. Mantovani A, Biswas SK, Galdiero MR, Sica A, Locati M. Macrophage plasticity and polarization in tissue repair and remodelling. J Pathol. 2013;229:176–85.
10. Shi J, Li Q, Sheng M, Zheng M, Yu M, Zhang L. The role of TLR4 in M1 macrophage-induced epithelial-mesenchymal transition of peritoneal mesothelial cells. Cell Physiol Biochem. 2016;40:1538–48.
11. Scalbert A, Manach C, Morand C, Rémésy C, Jiménez L. Dietary polyphenols and the prevention of diseases. Crit Rev Food Sci Nutr. 2005;45:287–306.
12. Salminen JP, Karonen M. Chemical ecology of tannins and other phenolics: we need a change in approach. Funct Ecol. 2011;25:325–38.
13. Pattarayan D, Sivanantham A, Krishnaswami V, Loganathan L, Palanichamy R, Natesan S, et al. Tannic acid attenuates TGF-β1-induced epithelial-to-mesenchymal transition by effectively intervening TGF-β signaling in lung epithelial cells. J Cell Physiol. 2018;233:2513–25.
14. Pattarayan D, Sivanantham A, Bethunaickan R, Palanichamy R, Rajasekaran S. Tannic acid modulates fibroblast proliferation and differentiation in response to pro-fibrotic stimuli. J Cell Biochem. 2018;119:6732–42.
15. Sivanantham A, Pattarayan D, Bethunaickan R, Kar A, Mahapatra SK, Thimmulappa RK, et al. Tannic acid protects against experimental acute lung injury through down-regulation of TLR4 and MAPK. J Cell Physiol. 2019;234:6463–76.
16. Chai WM, Wei QM, Deng WL, Zheng YL, Chen XY, Huang Q, et al. Anti-melanogenesis properties of condensed tannins from Vigna angularis seeds with potent antioxidant and DNA damage protection activities. Food Funct. 2019;10:99–111.
17. Koval A, Pieme CA, Queiroz EF, Ragusa S, Ahmed K, Blagodatski A, et al. Tannins from Syzygium guineense suppress Wnt signaling and proliferation of Wnt-dependent tumors through a direct effect on secreted Wnts. Cancer Lett. 2018;435:110–20.
18. Gourlay G, Constabel CP. Condensed tannins are inducible antioxidants and protect hybrid polar against oxidative stress. Tree Physiol. 2019;39:345–55.
19. Helmy IM, Azim AM. Efficacy of ImageJ in the assessment of apoptosis. Diag Pathol. 2012;7:15.
20. Wang Y, Su L, Morin MD, Jones BT, Whitby LR, Surakattula MM, et al. TLR4/MD-2 activation by a synthetic agonist with no similarity to LPS. Proc Natl Acad Sci USA. 2016;113:E884–93.
21. Maestro Suite, 2017, Version11.4.011, Schrodinger, LLC, NY.
22. Loganathan L, Muthusamy K. Investigation of drug interaction potentials and binding modes on direct renin inhibitors. A computational modeling studies. Lett Drug Des Discov. 2019;16:919–38.
23. Kawasaki K, Nogawa H, Nishijima M. Identification of mouse MD-2 residues important for forming the cell surface TLR4-MD-2 complex recognized by anti-TLR4-MD-2 antibodies, and for conferring LPS and taxol responsiveness on mouse TLR4 by alanine-scanning mutagenesis. J Immunol. 2003;170:413–20.
24. Park BS, Song DH, Kim HM, Choi BS, Lee H, Lee JO. The structural basis of lipopolysaccharide recognition by the TLR4-MD-2 complex. Nature. 2009;458:1191–5.
25. Santos AFM, Macedo LJA, Chaves MH, Castaneda ME, Merkoci A, Lima FCA, et al. Hybrid self-assembled materials constituted by ferromagnetic nanoparticles and tannic acid: a theoretical and experimental investigation. J Braz Chem Soc. 2016;27:727–34.
26. Kong J, Yu S. Fourier transform infrared spectroscopic analysis of protein secondary structures. Acta Biochim Biophys Sin. 2007;39:549–59.
27. Deng YR, Liu WB, Lian ZX, Li X, Hou X. Sorafenib inhibits macrophage-mediated epithelial-mesenchymal transition in hepatocellular carcinoma. Oncotarget. 2016;7:38292–305.
28. Wu KQ, Muratore CS, So EY, Sun C, Dubielecka PM, Reginato AM, et al. M1 macrophage-induced endothelial-to-mesenchymal transition promotes infantile hemangioma regression. Am J Pathol. 2017;187:2102–11.
29. Yeung OW, Lo CM, Ling CC, Qi X, Geng W, Li CX, et al. Alternatively activated (M2) macrophages promote tumour growth and invasiveness in hepatocellular carcinoma. J Hepatol. 2015;62:607–16.
30. Li Q, Lv LL, Wu M, Zhang XL, Liu H, Liu BC. Dexamethasone prevents monocyte-induced tubular epithelial-mesenchymal transition in HK-2 cells. J Cell Biochem. 2003;114:632–8.
31. Borthwick LA, Corris PA, Mahida R, Walker A, Gardner A, Suwara M, et al. TNFα from classically activated macrophages accentuates epithelial to mesenchymal transition in obliterative bronchiolitis. Am J Transplant. 2013;13:621–33.
32. Yamada M, Kuwano K, Maeyama T, Hamada N, Yoshimi M, Nakanishi Y, et al. Dual-immunohistochemistry provides little evidence for epithelial-mesenchymal transition in pulmonary fibrosis. Histochem Cell Biol. 2008;129:453–62.
33. Marmai C, Sutherland RE, Kim KK, Dolganov GM, Fang X, Kim SS, et al. Alveolar epithelial cells express mesenchymal proteins in patients with idiopathic pulmonary fibrosis. Am J Physiol Lung Cell Mol Physiol. 2011;301:L71–8.
34. Liang H, Gu Y, Li T, Zhang Y, Huangfu L, Hu M, et al. Integrated analyses identify the involvement of microRNA-26a in epithelial-mesenchymal transition during idiopathic pulmonary fibrosis. Cell Death Dis. 2014;5:e1238.
35. Tanjore H, Xu XC, Polosukhin VV, Degryse AL, Li B, Han W, et al. Contribution of epithelial-derived fibroblasts to bleomycin-induced lung fibrosis. Am J Respir Crit Care Med. 2009;180:657–65.
36. Inai T, Kobayashi J, Shibata Y. Claudin-1 contributes to the epithelial barrier function in MDCK cells. Eur J Cell Biol. 1999;78:849–55.
37. Shiozaki A, Bai XH, Shen-Tu G, Moodley S, Takeshita H, Fung SY, et al. Claudin 1 mediates TNFα-induced gene expression and cell migration in human lung carcinoma cells. PLoS One. 2012;7:e38049.
38. Fortier AM, Asselin E, Cadrin M. Keratin 8 and 18 loss in epithelial cancer cells increases collective cell migration and cisplatin sensitivity through claudin1 up-regulation. J Biol Chem. 2013;288:11555–71.
39. Grund EM, Kagan D, Tran CA, Zeitvogel A, Starzinski-Powitz A, Nataraja S, et al. Tumor necrosis factor-alpha regulates inflammatory and mesenchymal responses via mitogen-activated protein kinase kinase, p38, and nuclear factor kappaB in human endometriotic epithelial cells. Mol Pharmacol. 2008;73:1394–404.

40. Xiao J, Gong Y, Chen Y, Yu D, Wang X, Zhang X, et al. IL-6 promotes epithelial-to-mesenchymal transition of human peritoneal mesothelial cells possibly through the JAK2/STAT3 signaling pathway. Am J Physiol Renal Physiol. 2017;313:F310–8.
41. Lee SO, Yang X, Duan S, Tsai Y, Strojny LR, Keng P, et al. IL-6 promotes growth and epithelial-mesenchymal transition of CD133+ cells of non-small cell lung cancer. Oncotarget. 2016;7:6626–38.
42. Li S, Lu J, Chen Y, Xiong N, Li L, Zhang J, et al. MCP-1-induced ERK/GSK-3β/Snail signaling facilitates the epithelial-mesenchymal transition and promotes the migration of MCF-7 human breast carcinoma cells. Cell Mol Immunol. 2017;14:621–30.
43. Lee CH, Wu CL, Shiau AL. Toll-like receptor 4 signaling promotes tumor growth. J Immunother. 2010;33:73–82.
44. Sujitha S, Dinesh P, Rasool M. Berberine modulates ASK1 signaling mediated through TLR4/TRAF2 via upregulation of miR-23a. Toxicol Appl Pharmacol. 2018;359:34–46.
45. Rahimifard M, Maqbool F, Moeini-Nodeh S, Niaz K, Abdollahi M, Braidy N, et al. Targeting the TLR4 signaling pathway by polyphenols: A novel therapeutic strategy for neuroinflammation. Ageing Res Rev. 2017;36:11–9.
46. Joh EH, Gu W, Kim DH. Echinocystic acid ameliorates lung inflammation in mice and alveolar macrophages by inhibiting the binding of LPS to TLR4 in NF-kB and MAPK pathways. Biochem Pharmacol. 2012;84:40.
47. Zeng KW, Yu Q, Liao LX, Song FJ, Lv HN, Jiang Y, et al. Anti-neuroinflammatory effect of MC13, a novel coumarin compound from condiment murraya, through inhibiting lipopolysaccharide-Induced TRAF6-TAK1-NF-κB, P38/ERK MAPKS and Jak2-Stat1/Stat3 pathways. J Cell Biochem. 2015;116:1286–99.
48. Wang Y, Shan X, Dai Y, Jiang L, Chen G, Zhang Y, et al. Curcumin analog L48H37 prevents lipopolysaccharide-induced TLR4 signaling pathway activation and sepsis via targeting MD2. J Pharmacol Exp Ther. 2015;353:539–50.
49. Kim SY, Koo JE, Seo YJ, Tyagi N, Jeong E, Choi J, et al. Suppression of Toll-like receptor 4 activation by caffeic acid phenethyl ester is mediated by interference of LPS binding to MD2. Br J Pharmacol. 2013;168:1933–45.